Research Article | Vol. 29, No. 10 / 10 May 2021 / Optics Express 14773
Optics EXPRESS

Reconciliation of dipole emission with detailed balance rates for the simulation of luminescence and photon recycling in perovskite solar cells

URS AEBERHARD,[1,2,*] SIMON ZEDER,[1,3] AND BEAT RUHSTALLER[1,4]

[1] *Fluxim AG, Katharina-Sulzer-Platz 2, 8400 Winterthur, Switzerland*
[2] *Integrated Systems Laboratory, Dept. of Information Technology and Electrical Engineering, ETH Zurich, 8092 Zurich, Switzerland*
[3] *Photovoltaics and Thin Film Electronics Laboratory (PVLAB), Institute of Microengineering (IMT), EPFL, 2000 Neuchâtel, Switzerland*
[4] *Institute of Computational Physics, Zurich University of Applied Sciences (ZHAW), 8400 Winterthur, Switzerland*
[*] *urs.aeberhard@fluxim.com*

Abstract: A theoretical description of light emission, propagation and re-absorption in semiconductor multilayer stacks is derived based on the transverse Green's function of the electromagnetic field in the presence of a complex dielectric. The canonical dipole emission model is parametrized in terms of the local optical material constants and the local quasi-Fermi level splitting using the detailed balance relation between local absorption and emission rates. The framework obtained in this way is shown to reproduce the generalized Kirchhoff relations between the luminescent emission from metal halide perovskite slabs under uniform excitation and the slab absorptance of light with arbitrary angle of incidence. Use of the proper local density of transverse photon states in the local emission rate includes cavity effects in the generalized Planck law for internal spontaneous emission, which are neglected in the conventional Van Roosbroeck-Shockley formalism and avoids spurious divergencies due to non-radiative energy transfer via longitudinal modes. Finally, a consistent treatment of re-absorption provides the local rate of secondary photogeneration required for the consideration of photon recycling in an opto-electronic device simulator that includes the effects of charge transport.

1. Introduction

Owing to their large extinction coefficients, steep absorption edges, and long non-radiative lifetimes metal-halide perovskite semiconductors are used extensively for both, light-emitting and photovoltaic devices. The luminescence properties of these materials thereby play an essential role in the characterization of device performance. As a consequence of the sizable overlap between, absorption and emission spectra and of the operation close to the radiative limit [1,2], photon recycling effects due to re-absorption of internal emission [3–5] are found to have an impact on the device characteristics, in the form of an enhanced open-circuit voltage in solar cells [6] and of increased external quantum efficiency due to re-distribution of light from guided to leaky modes in light-emitting devices [7]. Since internal emission and re-absorption are not directly accessible to experimental observation, assessment and quantification of these processes relies strongly on modelling and simulation.

However, light emission is conventionally modeled based on theoretical frameworks that are different for LEDs and solar cells. While dipole emission models are routinely used to describe luminescence in organic light emitting diodes (OLED) [8–11], quantum dot LED [12] and inorganic optical waveguides [13,14], the modeling of luminescence from solar cells is

#424091 https://doi.org/10.1364/OE.424091
Journal © 2021 Received 15 Mar 2021; revised 18 Apr 2021; accepted 20 Apr 2021; published 28 Apr 2021

Optics EXPRESS

largely based on the reciprocity relations between, emission and global absorptance [15] (for photoluminescence - PL) or emission and external photovoltaic quantum efficiency [16] (for electroluminescence - EL). Indeed, the opto-electronic reciprocity theory has been applied successfully to solar cells based on silicon [17], CIGS [18], III-V semiconductors [19], organic materials [20–22] and metal-halide perovskites [1,23–28]. While this *global* detailed balance assessment of luminescence reflects both, the structure of the leaky optical modes in the absorber and the impact of photon recycling, the important aspect of a non-uniform density of photon states (DOS) due to cavity effects is absent in the standard formulation of the generalized Planck law conventionally used to describe the *local* radiative recombination rate in inorganic semiconductors based on the local values of absorption coefficient, refractive index and quasi-Fermi level splitting (QFLS) [29,30]. In the dipole model approach, on the other hand, the local emission rate is parametrized with an independent intrinsic spectrum (usually a measured single film PL spectrum), the local dipole density that is inferred either from the recombination current or from a charge transport model, and the effective dipole lifetime reflecting cavity effects [31]. Hence, while the relation of absorption and emission to the optical material constants is more consistent and obvious in the detailed balance approach, the impact of the actual local density of states is routinely considered only in the dipole emission models. As a notable exception, a formalism similar in spirit to the present work, but focused on near field effects on global emission of ultra-thin solar cells with uniform excitation, ideal carrier extraction and operating at the radiative limit was presented in Ref. [32].

The simulation-based assessment of the open-circuit voltage enhancement due to photon recycling in perovskite solar cells has therefore relied primarily on optical estimates in the detailed balance picture for internal and external emission [6,33]. The few works extending beyond the uniform photon DOS make use of rigorous solution of Maxwell's equations and dipole emission models to quantify internal and external emission [34,35], similar to the approach taken for the optical modeling of photon recycling in perovskite LED [7]. However, the latter approaches lack a rigorous connection to the detailed balance formalism. Furthermore, they are subject to the divergence issues encountered in any application of dipole emission in absorbing media, which originate in the non-radiative coupling to the evanescent quasi-static modes of the longitudinal field components at large in-plane photon momentum and necessitate the introduction of artificial non-absorbing environments around the radiating dipoles. Finally, and in contrast to the standard ray-optical consideration of photon recycling in wafer-based and thin film GaAs solar cells [36–38], the effects of photon recycling inferred from wave optical simulations of internal and external emission have not been propagated to the full device characteristics by using the corresponding radiative rates in a charge transport model. This, however, would be required in order to reproduce and analyze experimental device characteristics and project device performance in the presence of realistic non-radiative recombination losses at crucial interfaces that currently limit the efficiency of perovskite devices [39].

In this paper, we proceed further towards a unified theory of opto-electronic device operation, reconciling the two pictures of light emission introduced above via the derivation of a detailed balance parametrization of the local dipole emission rate, which then provides any global and local optical characteristics of relevance in terms of the local optical material constants, the local QFLS, and the regularized dyadic Green's function (GF) of the electromagnetic field. The approach is then applied to the simulation of light emission and re-absorption in methylammonium lead iodide (MAPI) slabs with and without metallic back reflector and is validated by comparing the global radiance with the predictions from the generalized Kirchhoff law. The local emission rate is formulated as a generalization of the Van Roosbroeck-Shockley (VRS) relation for arbitrary local photon DOS and shown to converge to the latter for slab thickness approaching the ray-optics limit, while deviating substantially for thin slabs. Finally, the local re-absorption rate is derived

Optics EXPRESS

and cast in a form that allows for straightforward integration into a charge transport model for full opto-electronic assessment of photon recycling effects on the solar cell device characteristics.

2. Green's function theory of dipole emission in absorbing media

2.1. Electromagnetic fields and Poynting vector

In classical electrodynamics, light emission from an excited semiconductor multilayer system is described by the time-averaged Poynting vector in terms of the transverse electric and magnetic fields $\boldsymbol{\mathcal{E}}$ and $\boldsymbol{\mathcal{H}}$, respectively [40]:

$$\langle \mathbf{S}(\mathbf{r},\omega)\rangle = \frac{1}{2}\Re\left[\boldsymbol{\mathcal{E}}(\mathbf{r},\omega)\times\boldsymbol{\mathcal{H}}^{*}(\mathbf{r},\omega)\right], \quad \boldsymbol{\mathcal{H}}(\mathbf{r},\omega) = \{i\omega\mu_0\mu\}^{-1}\nabla\times\boldsymbol{\mathcal{E}}(\mathbf{r},\omega), \tag{1}$$

where $\mathbf{r}$ is the position, ω the angular frequency, and μ (μ_0) the (vacuum) permeability. Hence, the central quantity of interest is the transverse electrical field in the presence of a source, which is related to the source current $\mathbf{j}$ via the corresponding dyadic Green's function $\overleftrightarrow{G}$:

$$\boldsymbol{\mathcal{E}}(\mathbf{r},\omega) = \boldsymbol{\mathcal{E}}_0(\mathbf{r},\omega) + i\omega\mu_0\mu\int \mathrm{d}^3r'\,\overleftrightarrow{G}(\mathbf{r},\mathbf{r}',\omega)\mathbf{j}(\mathbf{r}',\omega), \tag{2}$$

where $\boldsymbol{\mathcal{E}}_0(\mathbf{r},\omega)$ is the field in the source-free situation. In the case of a source consisting of a point dipole oscillating at position $\mathbf{r}_0$ with frequency ω, the current acquires the expression

$$\mathbf{j}(\mathbf{r},\omega) = -i\omega\mathbf{p}_0\delta(\mathbf{r}-\mathbf{r}_0), \tag{3}$$

where $\mathbf{p}_0$ is the dipole moment. Using this in (2) under the assumption of $\mu = 1$ and vanishing transverse fields in the source-free situation leads to the following (dipole) fields [31]

$$\boldsymbol{\mathcal{E}}(\mathbf{r},\omega) = \omega^2\mu_0\overleftrightarrow{G}(\mathbf{r},\mathbf{r}_0,\omega)\mathbf{p}_0, \quad \boldsymbol{\mathcal{H}}(\mathbf{r},\omega) = -i\omega\left[\nabla\times\overleftrightarrow{G}(\mathbf{r},\mathbf{r}_0,\omega)\right]\mathbf{p}_0, \tag{4}$$

and to the general expression of the Poynting vector in terms of the dyadic GF:

$$\langle \mathbf{S}(\mathbf{r},\omega)\rangle = -\frac{1}{2}\omega^3\mu_0\Im\left\{\left(\overleftrightarrow{G}(\mathbf{r},\mathbf{r}_0,\omega)\mathbf{p}_0\right)\times\left(\left[\nabla\times\overleftrightarrow{G}^{*}(\mathbf{r},\mathbf{r}_0,\omega)\right]\mathbf{p}_0^{*}\right)\right\}. \tag{5}$$

2.2. Energy dissipation rates

The total (radiative and non-radiative) rate of energy dissipation by a point dipole with unit polarization vector $\mathbf{n}_\mathrm{d}$ located at $\mathbf{r}_0$ in a *non-dispersive* medium is given by Poynting's theorem for harmonic current sources [31]:

$$\begin{aligned}\mathcal{P}(\mathbf{r}_0,\omega) &= -\frac{1}{2}\int \mathrm{d}^3r\,\Re\left\{\mathbf{j}^{*}(\mathbf{r},\omega)\cdot\boldsymbol{\mathcal{E}}(\mathbf{r},\omega)\right\} = \frac{\omega}{2}\Im\left\{\mathbf{p}_0^{*}\cdot\boldsymbol{\mathcal{E}}(\mathbf{r}_0,\omega)\right\}\\ &= \frac{\omega^3|\mathbf{p}_0|^2}{2c_0^2\varepsilon_0}\left[\mathbf{n}_\mathrm{d}\cdot\Im\left\{\overleftrightarrow{G}(\mathbf{r}_0,\mathbf{r}_0,\omega)\right\}\cdot\mathbf{n}_\mathrm{d}\right],\end{aligned} \tag{6}$$

where the term in square brackets is related to the partial LDOS and $\mu_0 = 1/(c_0^2\varepsilon_0)$ was used.

The rate of electromagnetic energy dissipation also provides the local generation rate due to re-absorption of internally emitted photons, as required for a quantitative assessment of photon recycling effects in the electronic device characteristics. According to the theory of electrodynamics in *dispersive* media characterized by the complex dielectric tensor $\overleftrightarrow{\varepsilon}$, the

Optics EXPRESS

dissipation due to absorption of electromagnetic (EM) energy amounts to [40] ($\Im\mu = 0$)

$$\mathcal{P}_{\mathrm{abs}}(\mathbf{r},\omega) = -\frac{1}{2}\omega\varepsilon_0\boldsymbol{\mathcal{E}}(\mathbf{r},\omega)\cdot\left(\Im\left[\overleftrightarrow{\varepsilon}(\mathbf{r},\omega)\right]\left[\boldsymbol{\mathcal{E}}(\mathbf{r},\omega)\right]^*\right). \tag{7}$$

For a field generated by an oscillating dipole with moment $\mathbf{p}_0 = p_0\mathbf{n}_\mathrm{d}$ located at $\mathbf{r}_0$, inserting Expr. (4) into the above equation yields

$$\mathcal{P}_{\mathrm{abs}}(\mathbf{r},\omega) = -\frac{1}{2}\omega^5\mu_0^2\varepsilon_0 p_0^2\left(\overleftrightarrow{G}(\mathbf{r},\mathbf{r}_0,\omega)\mathbf{n}_\mathrm{d}\right)\cdot\left(\Im\left[\overleftrightarrow{\varepsilon}(\mathbf{r},\omega)\right]\left[\overleftrightarrow{G}(\mathbf{r},\mathbf{r}_0,\omega)\right]^*\mathbf{n}_\mathrm{d}\right), \tag{8}$$

which provides the non-local relation between internal emission and re-absorption that is characteristic of the photon-recycling process.

2.3. Divergence issues and GF regularization

From the above considerations, the central quantity to evaluate for the assessment of the radiative rates is the real space GF. Since efficient numerical evaluation of the GF in stratified media proceeds in slab mode space, i.e., using a Fourier transform of the periodic dimension $\boldsymbol{\varrho} = \mathbf{r}_\parallel - \mathbf{r}'_\parallel$, the real space GF is obtained from an integration over in-plane momentum $\mathbf{q}_\parallel$:

$$\begin{aligned}\overleftrightarrow{G}(\mathbf{r},\mathbf{r}',\omega) \equiv \overleftrightarrow{G}(\boldsymbol{\varrho},z,z',\omega) &= \int\frac{\mathrm{d}^2q_\parallel}{(2\pi)^2}\overleftrightarrow{G}(\mathbf{q}_\parallel,z,z',\omega)e^{i\mathbf{q}_\parallel\cdot\boldsymbol{\varrho}}\\ &= \int_0^\infty\frac{\mathrm{d}q_\parallel}{(2\pi)}q_\parallel\overleftrightarrow{\mathcal{F}}(q_\parallel,\varrho)\overleftrightarrow{G}(q_\parallel,z,z',\omega)\end{aligned} \tag{9}$$

where $\mathcal{F}$ contains the integration over the angle between $\mathbf{q}_\parallel$ and $\boldsymbol{\varrho}$, which can be performed analytically [41,42]. As an example, the change in radiative lifetime due to cavity modes in MAPI is evaluated at $\hbar\omega = 1.65$ eV for a dipole with $\mathbf{n}_d = \hat{\mathbf{y}}$ located at $\mathbf{r}_0 = (0,0,z_0)$ in a non-absorbing layer sandwiched between two absorbing layers and surrounded by air. The layer thickness is 20 nm for all layers. The optical data of the MAPI is based on [43], but with a spectral shift introduced for band gap optimization with regard to application in perovskite-silicon tandems [44]. Evaluation of the effective radiative lifetime requires computation of $G_{yy}(\varrho,z_0,z_0,\omega)$ for $\varrho = 0$:

$$G_{yy}(0,z_0,z_0,\omega) = \int_0^\infty\frac{\mathrm{d}q_\parallel}{(2\pi)}\frac{q_\parallel}{2}\Big[G_{xx}(q_\parallel,z_0,z_0,\omega) + G_{yy}(q_\parallel,z_0,z_0,\omega)\Big]. \tag{10}$$

Inspection of the integrands as a function of z_0 and of the normalized in-plane photon momentum $q_\parallel/q_0$, where $q_0 = \omega/c_0$ with c_0 the vacuum speed of light, reveals a severe issue with divergencies in the xx- and zz-components related to TM-polarization, for $q_\parallel \to \infty$ and z_0 inside and in the proximity of the absorbing layers (upper row of Fig. 1). These divergencies are due to the non-radiative near-field transfer of energy via evanescent modes, which is related to the longitudinal (or quasi-static) components of the EM fields [45–47]. While consideration of this kind of energy transfer and the associated quenching of the luminescence might be justified for molecules in the vicinity of metal layers [48,49], the de-excitation of inorganic, non-excitonic semiconductors at low carrier density due to coupling to the EM fields proceeds primarily via the emission of transverse photons. Indeed, the *radiative* part of the energy dissipation rate (6) is related to the imaginary part of the *transverse* Green's function $\overleftrightarrow{G}_\mathrm{T}$ [13,46,50,51].

The transverse GF can be obtained via the generalized transverse delta function from generalized transverse solutions $\mathbf{f}$ of the Helmholtz equation, for which $\nabla\cdot\{\varepsilon(\mathbf{r})\mathbf{f}(\mathbf{r})\} = 0$ [52]. However, the computation is very involved, even for simple cases, where an analytical solution is possible [13,53]. We therefore follow Ref. [46] instead and approximate the transverse GF by subtraction of the purely longitudinal, non-retarded component $\overleftrightarrow{G}_\mathrm{L}$ from the full GF. In contrast to Ref. [46],

Optics EXPRESS

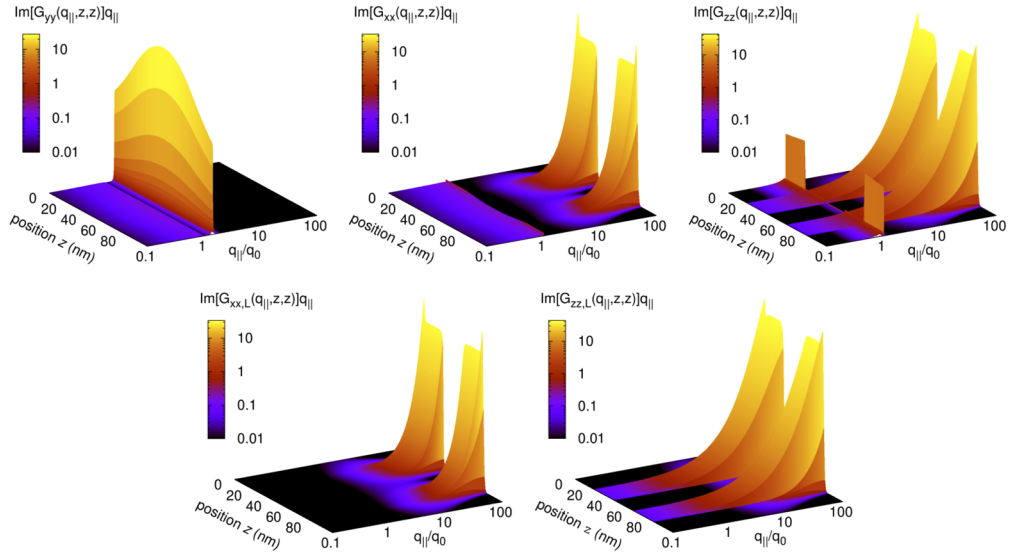

Fig. 1. (upper row) Imaginary part of the spatial diagonal of the full dyadic GF, which is related to the partial LDOS, as a function of polarization and normalized in-plane momentum $q_\parallel/q_0$. The structure consists of a non-absorbing layer sandwiched between two absorbing layers and surrounded by air. The thickness of the layers is 20 nm, and the optical material data for MAPI is used. The computation is performed for a photon energy of 1.65 eV, for which both significant absorption and emission is present. While the transverse *yy*-component features only radiative and wave guide modes, there are exponentially growing contributions to the *xx*- and *zz*-components that originate from non-radiative coupling to evanescent states in the absorbing layers. (lower row) Imaginary part of the spatial diagonal of the longitudinal/quasi-static GF components, which contains the divergent contributions to the full GF.

we use a Dyson equation approach to obtain consistently the full Dyadic GF and its quasi-static part.

The explicit expressions of the dyadic GF in free space $\overleftrightarrow{G}_0$ can be found in the literature, e.g. in Ref. [54]. Using this free space GF (and omitting the arguments $q_\parallel$, z, z' and ω), the equations for the full slab mode GF (including the effect of the absorbing medium) can be recast in the form of the Dyson equation ($\otimes \hat{=} \int dz$: tensor product includes integration over spatial arguments)

$$\overleftrightarrow{G} = \overleftrightarrow{G}_0 + \overleftrightarrow{G}_0 \otimes \overleftrightarrow{\Pi} \otimes \overleftrightarrow{G} \tag{11}$$

where for an *electronically* isotropic medium, the photon self-energy $\overleftrightarrow{\Pi}$ can be approximated by

$$\Pi_{ij}(\mathbf{q}_\parallel, z, z', \omega) = \frac{\omega^2}{c_0^2}\big(\varepsilon(z,\omega) - 1\big)\delta_{ij}\delta(z - z'), \tag{12}$$

and which can be solved either iteratively or, after rearranging, via direct matrix inversion.

The longitudinal GF is obtained from the solution of a similar Dyson equation employing the quasi-static component $\overleftrightarrow{G}_{0\mathrm{L}}$ of the free space GF which results from the full free-space GF by replacing the perpendicular wave vector $q_{z0} = \sqrt{q_0^2 - q_\parallel^2}$ with $iq_\parallel$ [46]. The lower row of Fig. 1 displays the imaginary part of the spatially diagonal entries of the longitudinal GF components, which are found to be identical to the diverging contributions in the full GF. Subtraction of this quasi-static part from the full GF therefore provides a GF that is well-behaved for large values

Optics EXPRESS

of the in-plane photon momentum. This is shown in Figs. 2(a) and (b) that display the spatial integration of the partial LDOS in the central layer as a function of in-plane momentum for a parallel [integrand in (10)] and a vertical dipole (z-component only), respectively. As can be inferred from Fig. 2(c) – displaying the physical in-plane momentum domain for a parallel dipole – the full GF result is in perfect agreement with the power dissipation based on the evaluation of the photonic LDOS as implemented in the established dipole emission simulation tool `Setfos` [55].

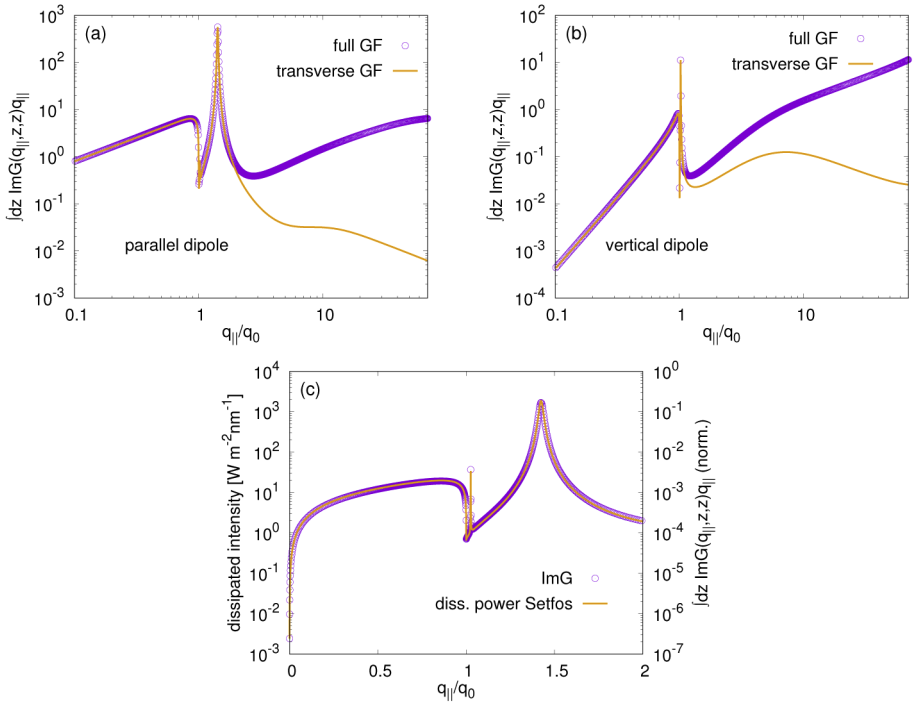

Fig. 2. Spatial integration of the partial LDOS in the central layer coupling to (a) a parallel dipole (x- and y-components) and (b) a vertical dipole (z-component only). Open symbols represent the full GF result that diverges for $q_\parallel \to \infty$, while the full line represents the result based on the transverse GF. (c) Comparison of the dissipated power from `Setfos` with the spatial integration of the imaginary part of the full GF, for the case of a parallel dipole.

More comprehensive microscopic treatments include both, radiative dissipation (via coupling to transverse GF) and non-radiative losses (from energy transfer via near-field Coulomb interaction) [56,57]. However, these works rely on the Huttner-Barnett model for the dielectric function of a polarizable medium, which does not depend on the transverse momentum and is designed for lossy dielectrics, not semiconductors. Furthermore, in the presence of absorption, the radiative decay rate is modified by local field effects that are related to the imaginary part of the dielectric constant [50]. Finally, the coupling of light and matter at large in-plane momenta is no longer described appropriately using the macroscopic continuum approximation of a dielectric medium, and the local photon self-energy (12) should be replaced by a non-local and momentum-dependent expression derived within a microscopic theory of electron-photon interaction [58–60].

3. Detailed balance parametrization of local and global emission

In the presence of a dipole distribution $\rho_d(z)$ (d: dipole orientation) and a normalized intrinsic emission spectrum $\mathcal{L}(\omega)$, the local and spectral rate of spontaneous emission based on the energy

Optics EXPRESS

dissipation rate (6) acquires the form

$$\begin{aligned}\mathcal{R}_{\mathrm{em}}(z,\omega) &\equiv \mathcal{P}_{\mathrm{em}}(z,\omega)/(\hbar\omega)\\ &= \frac{\omega^2}{2\hbar c_0^2\varepsilon_0} p_0^2(z)\mathcal{L}(\omega)\sum_{d\in\{x,y,z\}}\rho_d(z)\Big[\mathbf{n}_{\mathrm{d}}\cdot\Im\Big\{\overleftrightarrow{G}_{\mathrm{T}}(z,z,\omega)\Big\}\cdot\mathbf{n}_{\mathrm{d}}\Big].\end{aligned} \tag{13}$$

For an electronically isotropic material with average dipole density ρ, the local emission rate reduces to

$$\mathcal{R}_{\mathrm{em}}(z,\omega) = \frac{\omega^2}{2\hbar c_0^2\varepsilon_0} p_0^2(z)\rho(z)\mathcal{L}(\omega)\Im\Big[\mathrm{Tr}\,\overleftrightarrow{G}_{\mathrm{T}}(z,z,\omega)\Big] \tag{14}$$

where `Tr` denotes the trace over polarization indices.

On the other hand, the detailed balance relation between absorption and emission results in an expression of the spontaneous emission rate in terms of the local absorption coefficient or, more generally, the local and spectral values of the refractive index n_{r} and extinction coefficient κ – related to the dielectric function in (12) via $\varepsilon = (n_{\mathrm{r}} + i\kappa)^2$ – and the local value of the QFLS $\Delta\mu_{\mathrm{cv}}$, which for electronically isotropic materials can be written as follows [15,60]:

$$\mathcal{R}_{\mathrm{em}}(z,\omega) = \frac{4\omega^2}{c_0^2\pi\hbar} n_{\mathrm{r}}(z,\omega)\kappa(z,\omega)\Im\Big[\mathrm{Tr}\,\overleftrightarrow{G}_{\mathrm{T}}(z,z,\omega)\Big] f_{\mathrm{BE}}\big[\hbar\omega - \Delta\mu_{\mathrm{cv}}(z)\big], \tag{15}$$

where f_{BE} is the Bose-Einstein distribution function. This provides the relation

$$p_0^2(z)\rho(z)\mathcal{L}(\omega) = \frac{8}{\pi}\varepsilon_0 n_{\mathrm{r}}(z,\omega)\kappa(z,\omega) f_{\mathrm{BE}}\big[\hbar\omega - \Delta\mu_{\mathrm{cv}}(z)\big]. \tag{16}$$

The above identity can now be used to parametrize the dipole emission model in terms of the central quantities of the detailed balance theory.

3.1. Photon flux from internal emission expressed via the Poynting vector

As stated in Sec. 2, external emission - or global radiance - is evaluated from the Poynting vector for a given dipole distribution. In a laterally homogeneous and infinitely extended thin film where the emitters are assumed to be evenly distributed, only the perpendicular (i.e., z-) component of the Poynting vector is finite. The contributions S_z^α to the (spectral) Poynting vector normal to the slab from radiating dipoles with orientation α generating photons of energy $E_\gamma = \hbar\omega$ via internal emission due to an interband polarization related to the local QFLS $\Delta\mu_{\mathrm{cv}}$ can be expressed via Eqs. (5) and (16):

$$\begin{aligned}S_z^x(z,E_\gamma) = \frac{4E_\gamma^3}{\hbar^3 c_0^2\pi}\int \mathrm{d}z'\Big\{&n_{\mathrm{r}}(z',E_\gamma)\kappa(z',E_\gamma) f_{\mathrm{BE}}\big(E_\gamma - \Delta\mu_{\mathrm{cv}}(z')\big)\\ &\times\Im\int\frac{\mathrm{d}^2q_\parallel}{(2\pi)^2}\Big(G_{xx}(\mathbf{q}_\parallel,z,z',E_\gamma)\big[\partial_z G_{xx}(\mathbf{q}_\parallel,z,z',E_\gamma)\big]^*\\ &- iq_\parallel G_{xx}(\mathbf{q}_\parallel,z,z',E_\gamma)\big[G_{zx}(\mathbf{q}_\parallel,z,z',E_\gamma)\big]^*\Big)\Big\}\end{aligned} \tag{17}$$

and similar relations for S_z^y and S_z^z. For isotropic materials, the total photon flux is then the sum of the contributions of the different polarization orientations, $S_z = \sum_{\alpha\in\{x,y,z\}} S_z^\alpha \equiv S_z^{\mathrm{TE}} + S_z^{\mathrm{TM}}$, with $S_z^{\mathrm{TE}} = S_z^y$ and $S_z^{\mathrm{TM}} = S_z^x + S_z^z$. Figure 3(a) shows the TE and TM components of the photon flux at $E_\gamma = 1.65$ eV in a 100 nm MAPI layer subject to a uniform QFLS $\Delta\mu_{\mathrm{cv}} = 1.1$ eV. In Fig. 3(b) the flux components are displayed for the case where a metallic (Al) reflector is attached to the MAPI slab on the right side.

Optics EXPRESS

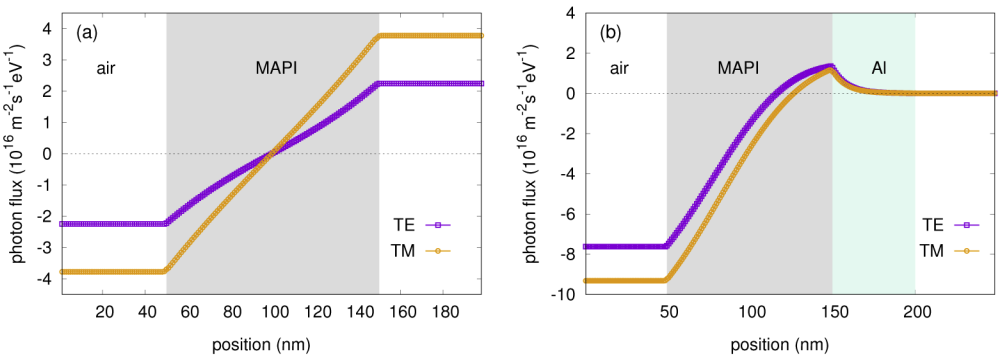

Fig. 3. Spatial evolution of the normal photon flux (TE and TM components) computed from the photon GF in a 100 nm MAPI slab subject to a uniform QFLS of 1.1 eV: (a) bare slab surrounded by air; (b) slab with metallic (Al) reflector attached at the right side.

3.2. Absorptance from the Green's function

While in stratified media, the absorptance of incident light as a function of in-plane photon momentum and photon energy - i.e., the *modal* absorptance - is conventionally evaluated in terms of a transfer matrix method (TMM), we choose here to express this quantity in terms of the photon Green's function in order to describe absorption and emission consistently on the basis of identical ingredients and within the same theoretical formalism. Evaluating the more general expressions for the absorptance in terms of the photon GF as derived within non-equilibrium quantum statistical mechanics [58,59,61] together with the photon-self energy expression in (12) yields (see Supplement 1 for an explicit derivation)

$$a_{\mathrm{TE}}(\mathbf{q}_\parallel, E_\gamma) = \frac{4E_\gamma^2}{(\hbar c_0)^2} \int \mathrm{d}z\, n_{\mathrm{r}}(z, E_\gamma)\kappa(z, E_\gamma)\Im\left[G_{\mathrm{vac},yy}(\mathbf{q}_\parallel, z, z, E_\gamma)\right], \tag{18}$$

$$a_{\mathrm{TM}}(\mathbf{q}_\parallel, E_\gamma) = \frac{4E_\gamma^2}{(\hbar c_0)^2} \int \mathrm{d}z\, n_{\mathrm{r}}(z, E_\gamma)\kappa(z, E_\gamma) \sum_{\mu=x,z} \Im\left[G_{\mathrm{vac},\mu\mu}(\mathbf{q}_\parallel, z, z, E_\gamma)\right], \tag{19}$$

where the vacuum-induced GF G_{vac} is given by [61,62] (momentum and energy arguments omitted)

$$\overleftrightarrow{G}_{\mathrm{vac}}(z, z') = \int \mathrm{d}z_1 \int \mathrm{d}z_2 \left[\overleftrightarrow{\varepsilon}\right]^{-1}(z, z_1) \cdot \left[\overleftrightarrow{G}_0(z_1, z_2) - \overleftrightarrow{G}_0^{\dagger}(z_1, z_2)\right] \cdot \left[\overleftrightarrow{\varepsilon}\right]^{-1,\dagger}(z_2, z') \tag{20}$$

with the inverse dielectric tensor

$$\left[\overleftrightarrow{\varepsilon}\right]^{-1}(z, z') = \int \mathrm{d}z_1\, \overleftrightarrow{G}(z, z_1)\overleftrightarrow{G}_0^{-1}(z_1, z') \tag{21}$$

and the free-field GF G_0. The comparison of the absorptance of the 100 nm MAPI slab evaluated from the above expression with the corresponding absorptance from `Setfos` is displayed in Fig. 4 and shows excellent agreement for both, different angles and polarization.

3.3. Generalized Kirchhoff law

With the above expressions for the Poynting vector and the absorptance, the generalized Kirchhoff relation [15] between slab absorptance and photon flux emitted from the the slab surfaces can be

Optics EXPRESS

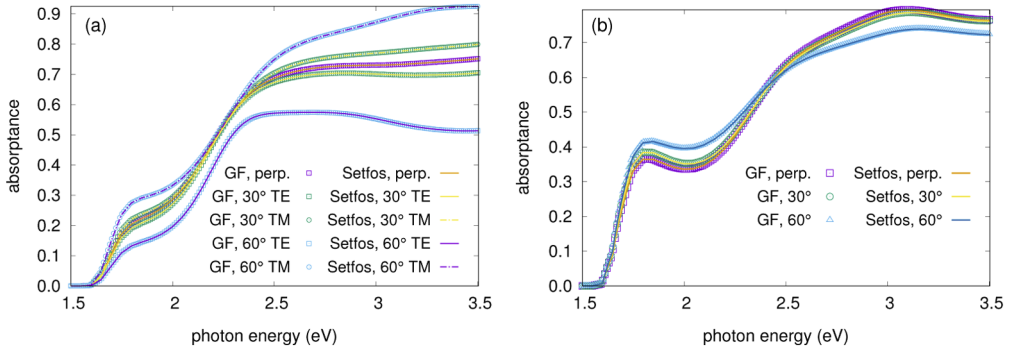

Fig. 4. Comparison of the absorptance as computed based on the photon GF with the result provided by the TMM solver implemented in `Setfos` [55], for different angles of incidence and polarization, of (a) a 100 nm MAPI slab in air, (b) a 100 nm MAPI slab with an Al back reflector (unpolarized).

verified for arbitrary (polar) angle θ of incidence/emission, as $\phi_{\mathrm{em}}(\theta, E_\gamma) = \sum_{z\in\partial V} S_z(\theta, E_\gamma)\hat{n}_z/E_\gamma$, where $\hat{\mathbf{n}}$ is the surface normal:

$$\Phi^{\lambda}_{\mathrm{em}}(E_\gamma) = 2\pi\phi_{\mathrm{bb}}(E_\gamma) f_{\mathrm{BE}}(E_\gamma - \Delta\mu_{\mathrm{cv}})/f_{\mathrm{BE}}(E_\gamma) \int_0^{\pi/2} \mathrm{d}\theta \sin(\theta)\cos(\theta) a_\lambda(\theta, E_\gamma), \tag{22}$$

$$\phi_{\mathrm{bb}}(E_\gamma) = \frac{E_\gamma^2}{4\pi^3\hbar^3 c_0^2} f_{\mathrm{BE}}(E_\gamma), \qquad (\lambda = \mathrm{TE}, \mathrm{TM}) \tag{23}$$

with ϕ_{bb} denoting the black-body photon flux. Using the relation $q_\parallel(\theta) = q_0 \sin(\theta)$, the emission spectrum can also be written in terms of an integration over transverse photon momentum:

$$\Phi^{\lambda}_{\mathrm{em}}(E_\gamma) = (\pi\hbar)^{-1} f_{\mathrm{BE}}(E_\gamma - \Delta\mu_{\mathrm{cv}}) \int_0^{q_0} \frac{\mathrm{d}q_\parallel}{2\pi} q_\parallel \, a_\lambda(\mathbf{q}_\parallel, E_\gamma), \qquad (\lambda = \mathrm{TE}, \mathrm{TM}) \tag{24}$$

which makes the connection to the modal absorptance. Figure 5(a) shows the perfect agreement between the emitted photon flux from absorptance (full line) and GF-based Poynting vector (open symbols) evaluated at the surface of a 100 nm thick MAPI layer with $\Delta\mu_{\mathrm{cv}} = 1.1$ eV. Figure 5(b)

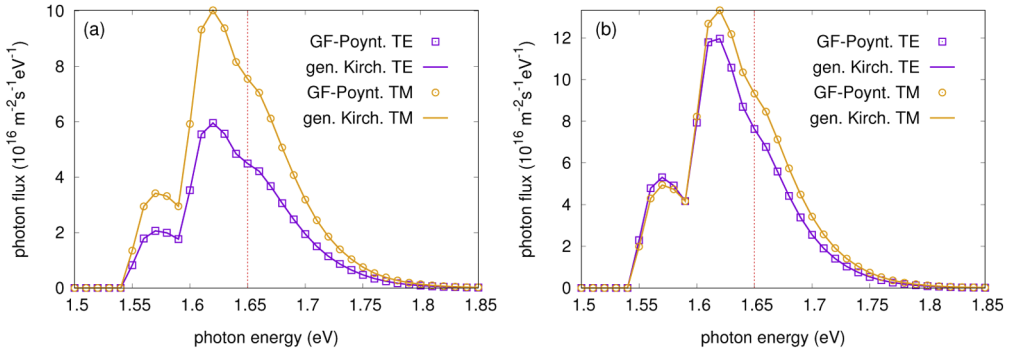

Fig. 5. Relation between photon flux from Poynting vector and from the absorptance via the generalized Kirchhoff law in a 100 nm MAPI slab subject to a uniform QFLS of 1.1 eV, (a) without and (b) with a metallic (Al) reflector. The red dotted line marks the photon energy for which the flux is shown in Fig. 3.

Optics EXPRESS

displays the situation in the case of the presence of a metallic (Al) reflector attached on the right side of the 100 nm MAPI slab, revealing again perfect coincidence of the fluxes from Poynting vector and generalized Kirchhoff law. To relate the spectral result to the spatially resolved picture displayed in Fig. 3, the red dotted lines mark the photon energy for which the flux is shown there. The apearance of a bump at the low-energy flank of the emission spectrum is related to the evolution of the extinction coefficient in the vicinity of the absorption edge (see Fig. S1 in Supplement 1), as low energy contributions are exponentially enhanced by the Bose-Einstein factor.

4. Local radiative rates - generalized Planck law and photon recycling

4.1. Local emission and re-absorption rates

After verification of the global reciprocity relation, expression (15) for the *local* emission rate is now to be compared to the VRS detailed balance theory [29]:

$$\mathcal{R}_{\mathrm{em}}^{\mathrm{VRS}}(z,E_\gamma)=\alpha(z,E_\gamma)\frac{n_{\mathrm{r}}^2(z,E_\gamma)E_\gamma^2}{\pi^2\hbar^3c_0^2}f_{\mathrm{BE}}\left[E_\gamma-\Delta\mu_{\mathrm{cv}}(z)\right], \tag{25}$$

where $\alpha=\kappa\cdot 2E_\gamma/(\hbar c_0)$ is the absorption coefficient. Expression (25) is reproduced as a special case of the general treatment introduced here by inserting the free field GF $\overleftrightarrow{G}_0$ (for uniform n_{r}) with $\Im\left[\mathrm{Tr}\left\{\overleftrightarrow{G}_0(z,z,E_\gamma)\right\}\right]=n_{\mathrm{r}}(z,E_\gamma)E_\gamma/(2\pi\hbar c_0)$ [31] in (15). Figure 6(a) shows the integral over energy $\mathcal{R}_{\mathrm{em}}(z)=\int \mathrm{d}E_\gamma\mathcal{R}_{\mathrm{em}}(z,E_\gamma)$ of the two spectral volume rates for a MAPI slab with uniform QFLS of 1.1 eV and thickness increasing from 100 nm to 1 um, which shows both the discrepancy at low absorber thickness and the convergence to the bulk limit. Comparison with the rate evaluated using the full GF - i.e., including the quasi-static contributions (dashed line) - at identical in-plane momentum integration limits given by the maximum value that still supports propagating modes confirms the relevance of the regularization procedure applied to obtain the transverse GF.

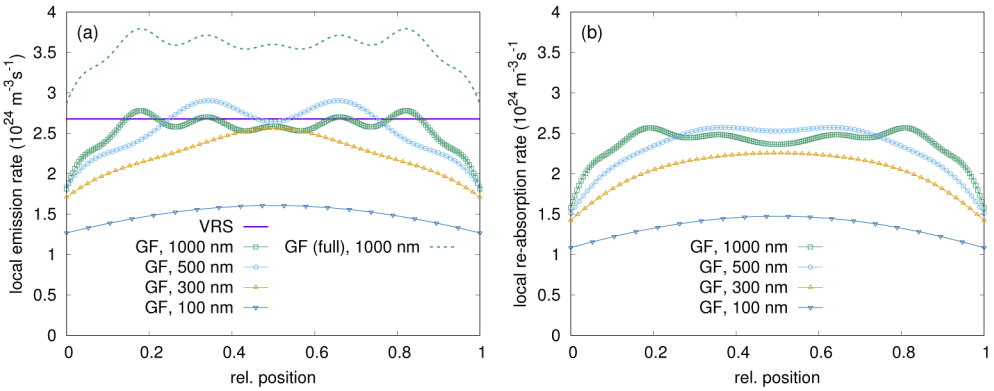

Fig. 6. (a) Local emission rate based on the detailed balance GF model in a MAPI slab of thickness ranging from 100 nm to 1000 nm and subject to a uniform QFLS of 1.1 eV. For increasing thickness, the rate converges to the value provided by the generalized Planck law based on the bulk absorption coefficient and free field LDOS. Use of the full instead of the transverse GF in the emission rate (at identical in-plane momentum integration limits) results in an overestimation of the emission rate due to the diverging non-radiative contributions (dashed line). (b) The local absorption rate shows both similar spatial variation and strength as the emission, which results in a sizable reduction of the net recombination rate.

Optics EXPRESS

For the quantification of the re-absorption, we consider again an isotropic stratified medium, i.e., $\overleftrightarrow{\varepsilon}(\mathbf{r},\omega) = \varepsilon(z,\omega)\overleftrightarrow{\delta}$, and a density of dipoles $\rho(z)$ with dispersion $\mathcal{L}(\omega)$, for which we can use the detailed balance parametrization given in Eq. (16). The local re-absorption rate then acquires the following form:

$$\mathcal{R}_{\rm abs}(z,E_\gamma) \equiv -\mathcal{P}_{\rm abs}(z,E_\gamma)/E_\gamma = \frac{8E_\gamma^4}{\pi\hbar^5 c_0^4} n_{\rm r}(z,E_\gamma)\kappa(z,E_\gamma)\int {\rm d}z' \Big\{ n_{\rm r}(z',E_\gamma)\kappa(z',E_\gamma) \times f_{\rm BE}[E_\gamma - \Delta\mu_{\rm cv}(z')] \sum_{\mu,\nu}\int \frac{{\rm d}^2 q_\parallel}{(2\pi)^2} |G_{\mu\nu}(\mathbf{q}_\parallel, z, z', E_\gamma)|^2 \Big\}. \tag{26}$$

Hence, unlike the local emission rate, the local re-absorption rate couples different points in space. This is a well-known issue in the quantitative evaluation of photon-recycling. Figure 6(b) shows the local re-absorption rate for the MAPI with uniform QFLS of 1.1 eV. Comparison with the local emission rate confirms the substantial reduction of the effective recombination translating into sizable $V_{\rm OC}$ gain. Figure 7(a) shows the comparison between the total (TE+TM) global radiance $\phi_{\rm em}^{\rm glob}$ from the cell (open symbols) and the spatial integration $\phi_{\rm em}^{\rm int}(E_\gamma) = \int {\rm d}z\, \mathcal{R}_{\rm em}(z,E_\gamma)$ of the local (TE+TM) internal emission rate (full line). The flux corresponding to the total emission rate is significantly larger than that for the emission into the loss cone ($\phi_{\rm em}^{\rm out}$, dashed line), which is inferred from the in-plane momentum threshold for modes propagating in air. To obtain the flux for the net emission ($\phi_{\rm em}^{\rm net}$, dotted line), the re-absorption rate is subtracted from the emission rate, which results in an emitted flux that agrees perfectly with the radiance from the Poynting vector or the generalized Kirchhoff law.

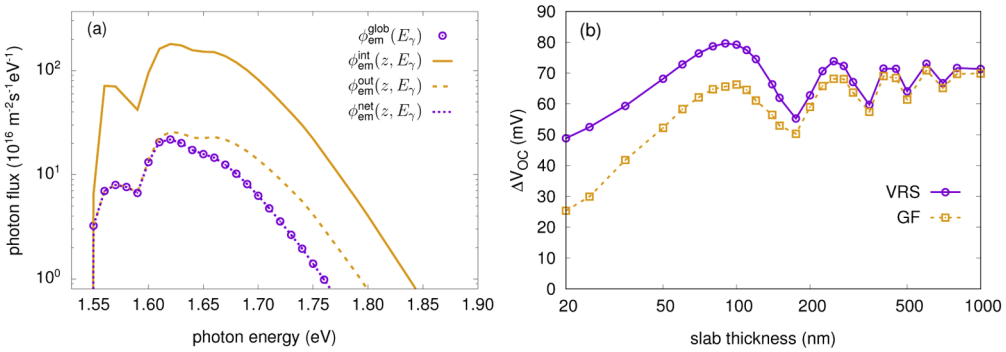

Fig. 7. (a) Comparison of the spatial integration of the total (full line) and net (dotted line) internal emission rate with the externally emitted photon flux (open symbols). Also shown is the flux due to emission into the optical loss cone (dashed line). (b) Implied open circuit voltage enhancement based on the relation between internal and external emission evaluated within the VRS and GF frameworks, respectively.

4.2. *Open-circuit voltage enhancement*

In an optical assessment of photon recycling at the radiative limit and for infinite mobility resulting in a uniform QFLS, $\Delta V_{\rm OC}^{\rm PR}$ has been expressed in terms of the radiative dark saturation currents for internal and external emission. Thereby, the generalized Kirchhoff law is used for the external emission and the internal emission is obtained from the spatial integration of the VRS emission rate [6]:

$$\Delta V_{\rm OC}^{\rm PR} \approx -\frac{k_{\rm B}T}{q}\ln(p_{\rm e}) \approx \frac{k_{\rm B}T}{q}\ln\left(\frac{J_{0,\rm rad}^{\rm int}}{J_{0,\rm rad}^{\rm ext}}\right), \tag{27}$$

Optics EXPRESS

$$J_{0,\mathrm{rad}}^{\mathrm{ext}} = q\int \mathrm{d}E_\gamma \left[\Phi_{\mathrm{em}}^{\mathrm{TE}}(E_\gamma) + \Phi_{\mathrm{em}}^{\mathrm{TM}}(E_\gamma)\right] = q\int \mathrm{d}E_\gamma\, \bar{a}(E_\gamma)\phi_{\mathrm{bb}}(E_\gamma), \tag{28}$$

$$J_{0,\mathrm{rad(VRS)}}^{\mathrm{int}} = q\int \mathrm{d}E_\gamma \int \mathrm{d}z\, \mathcal{R}_{\mathrm{em}}^{\mathrm{VRS}}(z,E_\gamma) = 4\pi q d\int \mathrm{d}E_\gamma\, n_{\mathrm{r}}^2(E_\gamma)\alpha(E_\gamma)\phi_{\mathrm{bb}}(E_\gamma), \tag{29}$$

where p_{e} is the probability of photon extraction, $\bar{a}(E_\gamma) = \sum_{\lambda=\mathrm{TE,TM}}\int \mathrm{d}\theta\, \sin(\theta)\cos(\theta)a_\lambda(E_\gamma,\theta)$, d is the thickness of the absorber and q is the electronic charge. The approximation sign is set due to the use of the Boltzmann approximation to the Bose-Einstein distribution that allows for the closed-form representation of $\Delta V_{\mathrm{OC}}^{\mathrm{PR}}$ and which is also used in the black-body photon flux ϕ_{bb} in the above equations. Using the same approximation, but starting from Expr. (15) for the generalized local emission rate, the dark saturation current from internal emission acquires the form

$$J_{0,\mathrm{rad(GF)}}^{\mathrm{int}} = q\int \mathrm{d}E_\gamma \int \mathrm{d}z\, \frac{2E_\gamma}{\pi\hbar^2 c_0} n_{\mathrm{r}}(z,E_\gamma)\alpha(z,E_\gamma)\exp\left(-\frac{E_\gamma}{k_{\mathrm{B}}T}\right)\Im\left[\mathrm{Tr}\overleftrightarrow{G}_{\mathrm{T}}(z,z,E_\gamma)\right], \tag{30}$$

which, in contrast to the VRS-based expression (29) and in consistency with the generalized Kirchhoff law (28) reflects the actual optical modes of the absorber. Figure 7(b) shows the evolution of $\Delta V_{\mathrm{OC}}^{\mathrm{PR}}$ with absorber layer thickness for the two approaches. In agreement with the comparison of the local emission rates in Fig. 6(a) and with the findings of previous investigations [35], $\Delta V_{\mathrm{OC}}^{\mathrm{PR}}$ inferred from the VRS with free field DOS overestimates internal emission at small absorber thickness but converges to the value obtained with the proper optical LDOS in the ray-optics limit, i.e., for slab thickness exceeding the wavelength of the emitted light.

When dealing with non-ideal systems, parasitic absorption is found to have a detrimental impact on the positive effect of PR [6,34,63]. In the present framework, parasitic absorption can be accounted for explicitly by evaluating the absorptance of layers that do not contribute to the generation of free charge carriers. Implicitly, parasitic absorption appears in the guise of light intensity attenuation due to interaction with absorbing, but non-generating components, most importantly, metallic reflectors. In fact, not only the loss involved in the reflection on metallic mirrors or the passage through absorbing contact layers is considered, but also the impact of plasmonic resonances on both, internal emission and re-absorption.

4.3. Coupling to charge transport

Coupling of the optical model to macroscopic charge transport on drift-diffusion level as implemented in standard opto-electronic device simulation tools [55,64] requires reformulation of the local rates for emission and re-absorption into corresponding terms for effective radiative recombination and secondary photogeneration. To this end, the standard Boltzmann approximation of the Bose-Einstein and Fermi-Dirac functions is used to obtain

$$f_{\mathrm{BE}}\left[E_\gamma - \Delta\mu_{\mathrm{cv}}(z)\right] \approx \exp\left[\left(\Delta\mu_{\mathrm{cv}}(z) - E_\gamma\right)/(k_{\mathrm{B}}T)\right] \approx \exp\left(-\frac{E_\gamma}{k_{\mathrm{B}}T}\right) n(z)p(z)/n_{\mathrm{i}}^2(z), \tag{31}$$

i.e., the local QFLS is expressed in terms of the local values of electron an hole densities n and p and intrinsic carrier concentration n_{i}. The radiative recombination term in the drift-diffusion equations is then written in the stardard form

$$\mathcal{R}_{\mathrm{rad}}(z) = \mathcal{B}_{\mathrm{rad}}(z)\left[n(z)p(z) - n_i^2(z)\right], \tag{32}$$

with the radiative recombination coefficient given by

$$\mathcal{B}_{\mathrm{rad}}^{\mathrm{VRS}}(z) = \frac{4\pi}{n_{\mathrm{i}}^2(z)}\int \mathrm{d}E_\gamma\, \alpha(z,E_\gamma)n_{\mathrm{r}}^2(z,E_\gamma)\phi_{\mathrm{bb}}(E_\gamma) \tag{33}$$

Optics EXPRESS

in the case of the VRS uniform LDOS approximation, and

$$\mathcal{B}_{\mathrm{rad}}^{\mathrm{GF}}(z) = \frac{2n_{\mathrm{i}}^{-2}(z)}{\pi\hbar^2 c_0} \int \mathrm{d}E_\gamma\, \alpha(z, E_\gamma) E_\gamma n_{\mathrm{r}}(z, E_\gamma) \exp\left(-\frac{E_\gamma}{k_{\mathrm{B}}T}\right) \Im\left[\mathrm{Tr}\overleftrightarrow{G}(z, z, E_\gamma)\right] \tag{34}$$

in the generalized version valid for arbitrary LDOS. Obviously, up to the factor n_{i}^{-2} these expressions for the recombination prefactor coincide with the integrands of the spatial integration in the expressions of the dark saturation currents for the internal emission as formulated in the previous section.

Expressions (26) – subject to the approximation (31) of the Bose-Einstein distribution – and (34) are suitable starting points for the numerical implementation that couples the optical to the electronic problem. Once the GF is computed, all that is required are the two functionals $\mathcal{F}_{\mathrm{em}}[\overleftrightarrow{G}]$ and $\mathcal{F}_{\mathrm{abs}}[\overleftrightarrow{G}]$, defined as follows:

$$\mathcal{F}_{\mathrm{em}}[\overleftrightarrow{G}](z, z, E_\gamma) \equiv \int \frac{\mathrm{d}^2 q_\parallel}{(2\pi)^2} \Im\left[\mathrm{Tr}\overleftrightarrow{G}(\mathbf{q}_\parallel, z, z, E_\gamma)\right], \tag{35}$$

$$\mathcal{F}_{\mathrm{abs}}[\overleftrightarrow{G}](z, z', E_\gamma) \equiv \int \frac{\mathrm{d}^2 q_\parallel}{(2\pi)^2} \sum_{\mu,\nu} \left|G_{\mu\nu}(\mathbf{q}_\parallel, z, z', E_\gamma)\right|^2. \tag{36}$$

These objects – as well as the corresponding emission coefficient (34) – have to be computed only once, while the QFLS (obtained from solution of the transport problem) and the re-absorption rate (26) have to be iterated until convergence is reached.

5. Conclusion

This work provides the formal derivation and numerical implementation of a novel approach to model the impact of a non-uniform density of electromagnetic modes on the luminescence in thin film photovoltaic absorbers that rigorously includes the effects of photon recycling beyond the ray-optical picture and avoids the notorious divergencies associated with emission in complex dielectrics. It unifies the theory of dipole emission with that of radiative rates from detailed balance and enables the consistent evaluation of internal and external emission under correct consideration of the EM modes, generalizing the Van Roosbroeck-Shockley formalism to arbitrary local photon density of states. Application to thin perovskite absorber films confirms the previously observed overestimation of the V_{OC} enhancement related to photon-recycling as obtained from uniform LDOS. The explicit formulation of local rates in dependence of the local quasi-Fermi level splitting paves the way to seamless integration with opto-electronic device simulation that propagates photon-recycling effects based on a full wave treatment from optical estimates to modification of the actual device characteristics of realistic solar cell architectures. Relevant directions of future work to extend the approach beyond the scope of the present article are towards, a rigorous inclusion of longitudinal energy transfer close to metallic layers into a non-radiative recombination term and the combination with scalar scattering theory for textured surfaces, which will allow for the simulation of tandem solar cells combining a thin perovskite absorber film with a random microtexture silicon wafer [44].

Funding. Horizon 2020 Framework Programme (953187–MUSICODE).

Acknowledgments. We would like to acknowledge stimulating discussions with Sandra Jenatsch and Balthasar Blülle from Fluxim as well as with Quentin Jeangros and Christophe Ballif from PV-Lab at EPFL.

Disclosures. The authors declare no conflicts of interest.

Data availability. Material and simulation data underlying the results presented in this paper are not publicly available at this time but may be obtained from the authors upon request.

Supplemental document. See Supplement 1 for supporting content.

Optics EXPRESS

References

1. K. Tvingstedt, O. Malinkiewicz, A. Baumann, C. Deibel, H. J. Snaith, V. Dyakonov, and H. J. Bolink, "Radiative efficiency of lead iodide based perovskite solar cells," Sci. Rep. **4**(1), 6071 (2015).
2. W. Tress, "Perovskite solar cells on the way to their radiative efficiency limit – insights into a success story of high open-circuit voltage and low recombination," Adv. Energy Mater. **7**(14), 1602358 (2017).
3. M. Saliba, W. Zhang, V. M. Burlakov, S. D. Stranks, Y. Sun, J. M. Ball, M. B. Johnston, A. Goriely, U. Wiesner, and H. J. Snaith, "Plasmonic-induced photon recycling in metal halide perovskite solar cells," Adv. Funct. Mater. **25**(31), 5038–5046 (2015).
4. L. M. Pazos-Outón, M. Szumilo, R. Lamboll, J. M. Richter, M. Crespo-Quesada, M. Abdi-Jalebi, H. J. Beeson, M. Vrucinic, M. Alsari, H. J. Snaith, B. Ehrler, R. H. Friend, and F. Deschler, "Photon recycling in lead iodide perovskite solar cells," Science **351**(6280), 1430–1433 (2016).
5. J. M. Richter, M. Abdi-Jalebi, A. Sadhanala, M. Tabachnyk, J. P. H. Rivett, L. M. Pazos-Outón, K. C. Gödel, M. Price, F. Deschler, and R. H. Friend, "Enhancing photoluminescence yields in lead halide perovskites by photon recycling and light out-coupling," Nat. Commun. **7**(1), 13941 (2016).
6. T. Kirchartz, F. Staub, and U. Rau, "Impact of photon recycling on the open-circuit voltage of metal halide perovskite solar cells," ACS Energy Lett. **1**(4), 731–739 (2016).
7. C. Cho, B. Zhao, G. D. Tainter, J.-Y. Lee, R. H. Friend, D. Di, F. Deschler, and N. C. Greenham, "The role of photon recycling in perovskite light-emitting diodes," Nat. Commun. **11**(1), 611 (2020).
8. H. Greiner and O. J. F. Martin, "Numerical modeling of light emission and propagation in organic LEDs using the Green's tensor," in *Organic Light-Emitting Materials and Devices VII*, vol. 5214 Z. H. Kafafi and P. A. Lane, eds., International Society for Optics and Photonics (SPIE, 2004), pp. 248–259.
9. K. Celebi, T. D. Heidel, and M. A. Baldo, "Simplified calculation of dipole energy transport in a multilayer stack using dyadic Green's functions," Opt. Express **15**(4), 1762–1772 (2007).
10. B. Perucco, N. A. Reinke, D. Rezzonico, M. Moos, and B. Ruhstaller, "Analysis of the emission profile in organic light-emitting devices," Opt. Express **18**(S2), A246–A260 (2010).
11. T. D. Schmidt, B. J. Scholz, C. Mayr, and W. Brütting, "Efficiency analysis of organic light-emitting diodes based on optical simulations," IEEE J. Sel. Top. Quantum Electron. **19**(5), 1–12 (2013).
12. R. Zhu, Z. Luo, and S.-T. Wu, "Light extraction analysis and enhancement in a quantum dot light emitting diode," Opt. Express **22**(S7), A1783–A1798 (2014).
13. T. Søndergaard and B. Tromborg, "General theory for spontaneous emission in active dielectric microstructures: Example of a fiber amplifier," Phys. Rev. A **64**(3), 033812 (2001).
14. Y. C. Jun, R. M. Briggs, H. A. Atwater, and M. L. Brongersma, "Broadband enhancement of light emission in silicon slot waveguides," Opt. Express **17**(9), 7479–7490 (2009).
15. P. Würfel, "The chemical potential of radiation," J. Phys. C: Solid State Phys. **15**(18), 3967–3985 (1982).
16. U. Rau, "Reciprocity relation between photovoltaic quantum efficiency and electroluminescent emission of solar cells," Phys. Rev. B **76**(8), 085303 (2007).
17. T. Kirchartz, A. Helbig, W. Reetz, M. Reuter, J. H. Werner, and U. Rau, "Reciprocity between electroluminescence and quantum efficiency used for the characterization of silicon solar cells," Prog. Photovoltaics **17**(6), 394–402 (2009).
18. T. Kirchartz and U. Rau, "Electroluminescence analysis of high efficiency Cu(In, Ga)Se_2 solar cells," J. Appl. Phys. **102**(10), 104510 (2007).
19. T. Kirchartz, U. Rau, M. Hermle, A. W. Bett, A. Helbig, and J. H. Werner, "Internal voltages in GaInP-GaInAs-Ge multijunction solar cells determined by electroluminescence measurements," Appl. Phys. Lett. **92**(12), 123502 (2008).
20. T. Kirchartz, J. Mattheis, and U. Rau, "Detailed balance theory of excitonic and bulk heterojunction solar cells," Phys. Rev. B **78**(23), 235320 (2008).
21. K. Vandewal, K. Tvingstedt, A. Gadisa, O. Inganas, and J. V. Manca, "On the origin of the open-circuit voltage of polymer-fullerene solar cells," Nat. Mater. **8**(11), 904–909 (2009).
22. T. Kirchartz, J. Nelson, and U. Rau, "Reciprocity between charge injection and extraction and its influence on the interpretation of electroluminescence spectra in organic solar cells," Phys. Rev. Appl. **5**(5), 054003 (2016).
23. W. Tress, N. Marinova, O. Inganäs, M. K. Nazeeruddin, S. M. Zakeeruddin, and M. Graetzel, "Predicting the open-circuit voltage of $CH_3NH_3PbI_3$ perovskite solar cells using electroluminescence and photovoltaic quantum efficiency spectra: the role of radiative and non-radiative recombination," Adv. Energy Mater. **5**(3), 1400812 (2015).
24. J. Yao, T. Kirchartz, M. S. Vezie, M. A. Faist, W. Gong, Z. He, H. Wu, J. Troughton, T. Watson, D. Bryant, and J. Nelson, "Quantifying losses in open-circuit voltage in solution-processable solar cells," Phys. Rev. Appl. **4**(1), 014020 (2015).
25. Z. Hameiri, A. M. Soufiani, M. K. Juhl, L. Jiang, F. Huang, Y.-B. Cheng, H. Kampwerth, J. W. Weber, M. A. Green, and T. Trupke, "Photoluminescence and electroluminescence imaging of perovskite solar cells," Prog. Photovoltaics **23**(12), 1697–1705 (2015).
26. G. El-Hajje, D. Ory, M. Paire, J.-F. Guillemoles, and L. Lombez, "Contactless characterization of metastable defects in Cu(In, Ga)Se_2 solar cells using time-resolved photoluminescence," Sol. Energy Mater. Sol. Cells **145**(Part 3), 462–467 (2016).

Optics EXPRESS

27. B. Hailegnaw, S. Paek, K. T. Cho, Y. Lee, F. Ongül, M. K. Nazeeruddin, and M. C. Scharber, "Optoelectronic properties of layered perovskite solar cells," Sol. RRL **3**(8), 1900126 (2019).
28. Z. Liu, L. Krückemeier, B. Krogmeier, B. Klingebiel, J. A. Márquez, S. Levcenko, S. Öz, S. Mathur, U. Rau, T. Unold, and T. Kirchartz, "Open-circuit voltages exceeding 1.26 V in planar methylammonium lead iodide perovskite solar cells," ACS Energy Lett. **4**(1), 110–117 (2019).
29. W. Van Roosbroeck and W. Shockley, "Photon-radiative recombination of electrons and holes in germanium," Phys. Rev. **94**(6), 1558–1560 (1954).
30. G. Lasher and F. Stern, "Spontaneous and stimulated recombination radiation in semiconductors," Phys. Rev. **133**(2A), A553–A563 (1964).
31. L. Novotny and B. Hecht, *Principles of Nano-Optics* (Cambridge University Press, 2006).
32. A. Niv, M. Gharghi, C. Gladden, O. D. Miller, and X. Zhang, "Near-Field Electromagnetic Theory for Thin Solar Cells," Phys. Rev. Lett. **109**(13), 138701 (2012).
33. A. Martí, J. L. Balenzategui, and R. F. Reyna, "Photon recycling and shockley's diode equation," J. Appl. Phys. **82**(8), 4067–4075 (1997).
34. M. G. Abebe, A. Abass, G. Gomard, L. Zschiedrich, U. Lemmer, B. S. Richards, C. Rockstuhl, and U. W. Paetzold, "Rigorous wave-optical treatment of photon recycling in thermodynamics of photovoltaics: Perovskite thin-film solar cells," Phys. Rev. B **98**(7), 075141 (2018).
35. S. Nanz, R. Schmager, M. G. Abebe, C. Willig, A. Wickberg, A. Abass, G. Gomard, M. Wegener, U. W. Paetzold, and C. Rockstuhl, "Photon recycling in nanopatterned perovskite thin-films for photovoltaic applications," APL Photonics **4**(7), 076104 (2019).
36. S. Durbin and J. Gray, "Numerical modeling of photon recycling in solar cells," IEEE Trans. Electron Devices **41**(2), 239–245 (1994).
37. G. Létay, M. Hermle, and A. W. Bett, "Simulating single-junction GaAs solar cells including photon recycling," Prog. Photovoltaics **14**(8), 683–696 (2006).
38. A. W. Walker, O. Höhn, D. N. Micha, B. Bläsi, A. W. Bett, and F. Dimroth, "Impact of photon recycling on GaAs solar cell designs," IEEE J. Photovoltaics **5**(6), 1636–1645 (2015).
39. M. Stolterfoht, C. M. Wolff, J. A. Marquez, S. Zhang, C. J. Hages, D. Rothhardt, S. Albrecht, P. L. Burn, P. Meredith, T. Unold, and D. Neher, "Visualization and suppression of interfacial recombination for high-efficiency large-area pin perovskite solar cells," Nat. Energy **3**(10), 847–854 (2018).
40. J. Jackson, *Classical Electrodynamics* (John Wiley & Sons, 1998).
41. M. Paulus, P. Gay-Balmaz, and O. J. F. Martin, "Accurate and efficient computation of the Green's tensor for stratified media," Phys. Rev. E **62**(4), 5797–5807 (2000).
42. P. Johansson, "Electromagnetic Green's function for layered systems: Applications to nanohole interactions in thin metal films," Phys. Rev. B **83**(19), 195408 (2011).
43. P. Löper, M. Stuckelberger, B. Niesen, J. Werner, M. Filipic, S.-J. Moon, J.-H. Yum, M. Topic, S. De Wolf, and C. Ballif, "Complex refractive index spectra of $CH_3NH_3PbI_3$ perovskite thin films determined by spectroscopic ellipsometry and spectrophotometry," J. Phys. Chem. Lett. **6**(1), 66–71 (2015).
44. S. Altazin, L. Stepanova, J. Werner, B. Niesen, C. Ballif, and B. Ruhstaller, "Design of perovskite/crystalline-silicon monolithic tandem solar cells," Opt. Express **26**(10), A579–A590 (2018).
45. R. R. Chance, A. Prock, and R. Silbey, "Lifetime of an emitting molecule near a partially reflecting surface," J. Chem. Phys. **60**(7), 2744–2748 (1974).
46. M. S. Tomaš and Z. Lenac, "Decay of excited molecules in absorbing planar cavities," Phys. Rev. A **56**(5), 4197–4206 (1997).
47. K. A. Neyts, "Simulation of light emission from thin-film microcavities," J. Opt. Soc. Am. A **15**(4), 962–971 (1998).
48. B. Perucco, N. Reinke, D. Rezzonico, E. Knapp, S. Harkema, and B. Ruhstaller, "On the exciton profile in OLEDs - seamless optical and electrical modeling," Org. Electron. **13**(10), 1827–1835 (2012).
49. M. Regnat, K. P. Pernstich, and B. Ruhstaller, "Influence of the bias-dependent emission zone on exciton quenching and OLED efficiency," Org. Electron. **70**, 219–226 (2019).
50. S. M. Barnett, B. Huttner, and R. Loudon, "Spontaneous emission in absorbing dielectric media," Phys. Rev. Lett. **68**(25), 3698–3701 (1992).
51. S. Scheel, L. Knöll, and D.-G. Welsch, "Spontaneous decay of an excited atom in an absorbing dielectric," Phys. Rev. A **60**(5), 4094–4104 (1999).
52. R. J. Glauber and M. Lewenstein, "Quantum optics of dielectric media," Phys. Rev. A **43**(1), 467–491 (1991).
53. A. M. C. Reyes and C. Eberlein, "Completeness of evanescent modes in layered dielectrics," Phys. Rev. A **79**(4), 043834 (2009).
54. V. Despoja, M. Šunjić, and L. Marušić, "Propagators and spectra of surface polaritons in metallic slabs: Effects of quantum-mechanical nonlocality," Phys. Rev. B **80**(7), 075410 (2009).
55. Fluxim AG, *Setfos v5.1*. https://www.fluxim.com/setfos-intro.
56. M. S. Yeung and T. K. Gustafson, "Spontaneous emission near an absorbing dielectric surface," Phys. Rev. A **54**(6), 5227–5242 (1996).
57. C. Eberlein and R. Zietal, "Quantum electrodynamics near a dispersive and absorbing dielectric," Phys. Rev. A **86**(2), 022111 (2012).

Optics EXPRESS

58. U. Aeberhard, "Quantum-kinetic theory of steady-state photocurrent generation in thin films: Coherent versus incoherent coupling," Phys. Rev. B **89**(11), 115303 (2014).
59. U. Aeberhard, "Photon Green's functions for a consistent theory of absorption and emission in nanostructure-based solar cell devices," Opt. Quantum Electron. **46**(6), 791–796 (2014).
60. U. Aeberhard and U. Rau, "Microscopic perspective on photovoltaic reciprocity in ultrathin solar cells," Phys. Rev. Lett. **118**(24), 247702 (2017).
61. F. Richter, M. Florian, and K. Henneberger, "Generalized radiation law for excited media in a nonequilibrium steady state," Phys. Rev. B **78**(20), 205114 (2008).
62. K. Henneberger and F. Richter, "Exact property of the nonequilibrium photon Green function for bounded media," Phys. Rev. A **80**(1), 013807 (2009).
63. U. Rau, U. W. Paetzold, and T. Kirchartz, "Thermodynamics of light management in photovoltaic devices," Phys. Rev. B **90**(3), 035211 (2014).
64. B. Ruhstaller, E. Knapp, B. Perucco, N. Reinke, D. Rezzonico, and F. Müller, "Advanced numerical simulation of organic light-emitting devices," in *Optoelectronic Devices and Properties*, O. Sergiyenko, ed. (IntechOpen, Rijeka, 2011), chap. 21.